NANO · MICRO small
www.small-journal.com

Intermittent Fasting Primes the Tumor Microenvironment and Improves Nanomedicine Delivery in Hepatocellular Carcinoma

Svea Becker, Jeffrey Momoh, Ilaria Biancacci, Diana Möckel, Qingbi Wang, Jan-Niklas May, Huan Su, Lena Susanna Candels, Marie-Luise Berres, Fabian Kiessling, Maximilian Hatting, Twan Lammers, and Christian Trautwein**

Fasting has many health benefits, including reduced chemotherapy toxicity and improved efficacy. It is unclear how fasting affects the tumor microenvironment (TME) and tumor-targeted drug delivery. Here the effects of intermittent (IF) and short-term (STF) fasting are investigated on tumor growth, TME composition, and liposome delivery in allogeneic hepatocellular carcinoma (HCC) mouse models. To this end, mice are inoculated either subcutaneously or intrahepatically with Hep-55.1C cells and subjected to IF for 24 d or to STF for 1 d. IF but not STF significantly slows down tumor growth. IF increases tumor vascularization and decreases collagen density, resulting in improved liposome delivery. In vitro, fasting furthermore promotes the tumor cell uptake of liposomes. These results demonstrate that IF shapes the TME in HCC towards enhanced drug delivery. Finally, when combining IF with liposomal doxorubicin treatment, the antitumor efficacy of nanochemotherapy is found to be increased, while systemic side effects are reduced. Altogether, these findings exemplify that the beneficial effects of fasting on anticancer therapy outcomes go beyond modulating metabolism at the molecular level.

1. Introduction

In recent years, fasting has been shown to have beneficial effects on both the efficacy and the tolerability of anticancer therapy.[1–4] By stimulating systemic and intracellular metabolism, it makes tumor cells more susceptible to therapy.[5,6] It furthermore remodels intratumoral immunity so that antineoplastic treatments benefit from activated antitumor immune programs.[3] Fasting has also been shown to improve the response to hormone therapy in breast cancer, demonstrating its utility as an adjuvant therapy.[2]

Many mechanisms have been proposed to explain the benefits of fasting in tumor therapy. For example, tumor cells rely on the Warburg effect to maintain their high proliferative activity. Here, the cells engage in anabolic pathways, such as glycolysis, despite their energetic inefficiency compared to oxidative means. This causes tumor cells to become more dependent on an increased external glucose supply.[7–10] Additionally, they lack compensatory maintenance mechanisms such as autophagy, which enhances the susceptibility of the tumor cells to systematic nutrient deprivation by fasting.[11] Reducing glucose levels creates an "anti-Warburg" effect, forcing tumor cells to down-regulate anaerobic glycolysis and revert back to oxidative phosphorylation resulting in oxidative stress and apoptosis.[10] This is further reinforced by oncogenes preventing the activation of stress resistance mechanisms and causing cells to maintain a high proliferation level.[9,10] Due to these mechanisms tumor

S. Becker, Q. Wang, H. Su, L. S. Candels, M.-L. Berres, M. Hatting, C. Trautwein
Clinic for Gastroenterology, Metabolic Disorders, and Internal Intensive Medicine (Med III)
University Hospital RWTH Aachen
52074 Aachen, Germany
E-mail: ctrautwein@ukaachen.de

S. Becker, J. Momoh, I. Biancacci, D. Möckel, J.-N. May, F. Kiessling, T. Lammers
Institute for Experimental Molecular Imaging (ExMI)
University Hospital RWTH Aachen
52074 Aachen, Germany
E-mail: tlammers@ukaachen.de

The ORCID identification number(s) for the author(s) of this article can be found under https://doi.org/10.1002/smll.202208042

DOI: 10.1002/smll.202208042

cells become more sensitive toward DNA damage and oxidative stress upon fasting, which is defined as differential stress sensitization (DSS).[5,9,10] This leads to an increased sensitivity towards chemotherapy, allowing equal therapeutic effects at lower doses of chemotherapy with reduced risk of side effects.[4,9]

An additional and thus far unstudied mechanism through which fasting can improve tumor treatment might be via modulation of the tumor microenvironment (TME) and tumor-directed drug delivery. Important components of the TME include tumor vascularization, infiltration of immune cells and extracellular matrix (ECM) characteristics, which are known to affect cancer cell survival, local invasion, and metastatic dissemination.[6] However, they are also known to have an effect on tumor-directed delivery with tumor vascularization directly affecting perfusion and delivery,[12] immune cells acting as a slow drug release reservoir,[13] and the ECM functioning as a barrier for drug transport into tumor tissue.[14] Delivery of conventional chemotherapeutics often exhibits unfavorable distribution, poor target selectivity and high toxicity to nontargeted tissues due to their systemic application and low specificity.[15] These issues can cause dose-limiting side effects over time hindering their clinical application, and creating the need for refined treatment options.[16] Improving drug delivery can be achieved through nanomedicines, which uses physical and biological characteristics of nanocarriers to increase selective accumulation at tumor sites. Organic nanoparticles like liposomes can help deliver drugs directly into cells, avoiding high concentrations of free drugs and reducing adverse reactions.[15] As the TME and tumor-directed delivery of nanoparticles might be influenced by fasting, it could provide a useful strategy to further improve nanomedicine therapies.

Nanomedicine has been progressively advancing, making it an ever more prominent approach in many tumor entities including liver tumors such as hepatocellular carcinoma (HCC).[17,18] Conventional treatment options in advanced or irresectable HCC are typically limited to systemic and local ablative therapies.[19,20] To improve treatment outcomes, combining radiofrequency ablation with nanotherapeutics like Thermodox (lyso-thermosensitive liposomal doxorubicin) has been explored.[21] Despite strong nanoparticle accumulation in the liver in general, difficulties of selectively targeting tumoral hepatocytes in HCC remain. As an example, a rapid sequestration of nanocarriers by macrophages can influence nanomedicine tumor accumulation, compromising therapeutic efficacy.[17] Increasing target localization and specificity towards tumoral hepatocytes is a crucial aspect to improve (nano-) pharmacotherapies in HCC, which may be achieved by concomitant fasting.

Here, we investigated the effect of short-term fasting (STF) and intermittent fasting (IF) on tumor growth of hepatomas, TME composition and tumor-targeted liposome delivery. Notably, we find that IF but not STF significantly primes the TME and positively affects liposome tumor targeting. Moreover, studying the in vitro impact of fasting on liposome internalization by Hep-55.1C and Hepa1.6 cells reveals significantly enhanced uptake of liposomes upon fasting-mimicking treatments. We further demonstrate an increased chemotherapeutic effect of liposomal doxorubicin in intermittently fasted mice. Due to the beneficial effects of fasting at both the cellular and systemic level, it is considered a potent and useful adjuvant to improve drug delivery and enhance anticancer (nano-) therapy.

2. Results

2.1. IF Reduces Subcutaneous Tumor Growth and Improves Liposome Accumulation

To study the impact of fasting on tumor-targeted drug delivery, mice were inoculated subcutaneously with Hep-55.1C cells and divided into three groups. The control group (ctrl) had ad libitum access to food and water. Short-term fasted mice (STF) were fed ad libitum, except on day 21, when they were fasted for 12 h. Intermittently fasted (IF) mice alternated between 12 h of fasting and 12 h of ad libitum food supply for 24 consecutive days. Mice were fasted overnight, i.e., during their active phase (**Figure 1**A), following previously established procedures.[10,22] The effects of fasting on tumor growth were monitored by micro-computed tomography (μCT). On day 22, Cy7-labeled liposomes were administered i.v. to all mice. Their biodistribution and tumor accumulation were measured up to 72 h postinjection (p.i.), by combined μCT and fluorescence tomography (μCT-FLT; Figure 1B).

IF initially resulted in significant weight loss (Figure 1C), but after 10 d mice were acclimatized, and no significant weight differences could be observed compared to the ad libitum-fed mice. Mice subjected to STF lost weight significantly on day 22, but this was found to be regained on the following day upon refeeding (Figure 1C). Consistent with previous observations about the impact of fasting on tumor growth,[23,24] we found via μCT imaging that tumor growth was significantly suppressed upon IF compared to STF and control groups (Figure 1D,E).

We next studied the effect of IF and STF on tumor-directed drug delivery. To this end, after 3 weeks (IF) or 1 d (STF) of fasting, Cy7-labeled liposomes were administered i.v., and their biodistribution and tumor accumulation were visualized and quantified via μCT-FLT at 0.25, 4, 24, 48, and 72 h p.i. (Figure 1F). At early time points (0.25 and 4 h p.i.), liposome localization in all three groups was most pronounced in well-perfused organs, including heart, liver and spleen (Figure S1, Supporting Information). Liposome tumor accumulation started to become prominent at later time points, showing a clearly distinct pattern between controls and the different fasting conditions (Figure 1G). We observed a significantly higher tumor accumulation of liposomes in the IF group, with 12.8%ID/g compared to 2.5%ID/g in the control group ($P < 0.0001$) at the 48-h timepoint. This increase was still evident 72 h after injection ($P = 0.005$). Mice fasted just once (STF) before liposome injection also showed a higher level of liposome tumor accumulation compared to control animals, but this difference was not statistically significant ($P = 0.15$ at 72 h).

We confirmed the effect of IF on liposome tumor accumulation in *ex vivo* tissue sections. To stain for areas positive of PEG-liposomes, we employed anti-PEG antibodies providing a strong signal to detect intracellular liposomes (Figure 1H). In line with the in vivo findings, we found that IF substantially increases the accumulation of pegylated liposomes in tumors as compared to control and STF, as evidenced by enhancements of relative PEG^+ area fraction of 7.04% for IF ($P = 0.001$) and 1.90 for STF ($P = 0.002$).

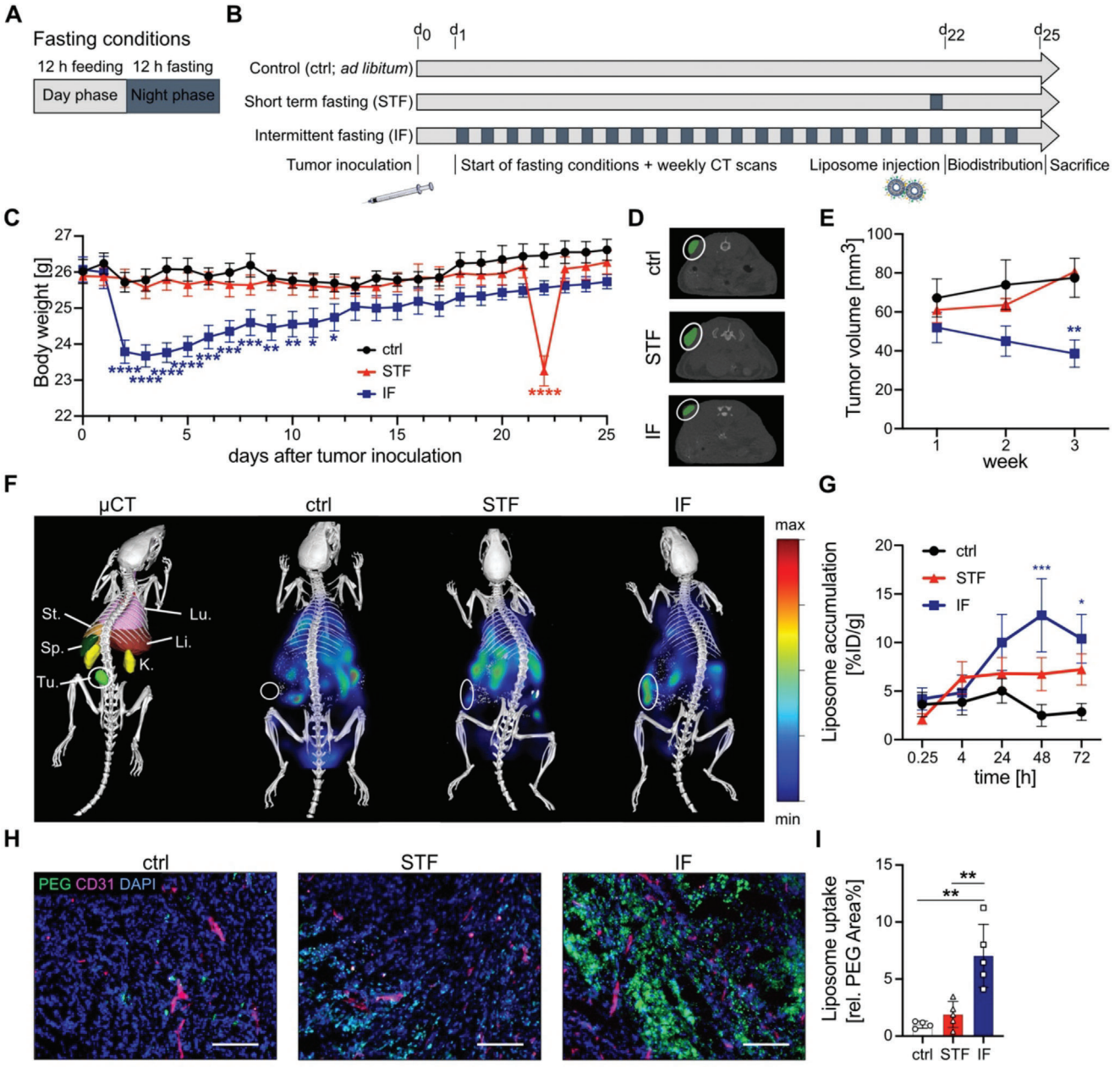

Figure 1. Intermittent fasting increases liposome accumulation in subcutaneous tumors. A,B) Schematic overview of fasting conditions and experimental timeline. C) The body weight was measured every morning. IF was initiated two days after tumor inoculation. On day 22, STF was performed for 12 h. Values represent mean ± SEM (ctrl $n = 10$, STF $n = 11$, IF $n = 11$ mice). Two-way ANOVA and Dunnett's multiple comparisons test were used for statistical analysis. D) Representative weekly µCT scans shown in 2D cross-sectional transverse plane. The tumor is color-coded in green and its location is indicated with a white circle. E) CT scans showed a significant reduction in tumor growth upon IF. Values represent mean ± SEM (ctrl $n = 4$, STF $n = 5$, IF $n = 5$ mice). Two-way ANOVA and Dunnett's multiple comparisons test were used. F) Liposome biodistribution and tumor accumulation were assessed via µCT-FLT shown as 3D reconstruction. Organ segmentation was performed using µCT. Lu. = lungs, Li. = liver, St. = stomach, Sp. = spleen, K. = kidneys, Tu. = tumor. The tumor location is indicated with a white circle. Representative µCT-FLT scans are shown for 72 h post i.v. injection of Cy7-labeled liposomes. G) Quantification of liposome distribution demonstrates a significantly higher tumor accumulation upon IF. Values represent mean ± SEM (ctrl $n = 10$, STF $n = 11$, IF $n = 11$ mice). Two-way ANOVA and Dunnett's multiple comparisons test were used. H) Representative fluorescence microscopy images showing liposome distribution in tumors (anti-PEG staining), blood vessels (CD31), and cell nuclei (DAPI) for control and fasting groups. The scale bar indicates 25 µm. I) Analysis of liposome tumor accumulation upon fasting, based on quantification of the microscopy images. Values represent mean ± SD. Statistical analysis based on one-way ANOVA and Tukey's multiple comparisons test. ****$P < 0.0001$, ***$P < 0.001$, **$P < 0.01$, *$P < 0.05$, ns = not significant ($P > 0.05$). Figure was created with Biorender.

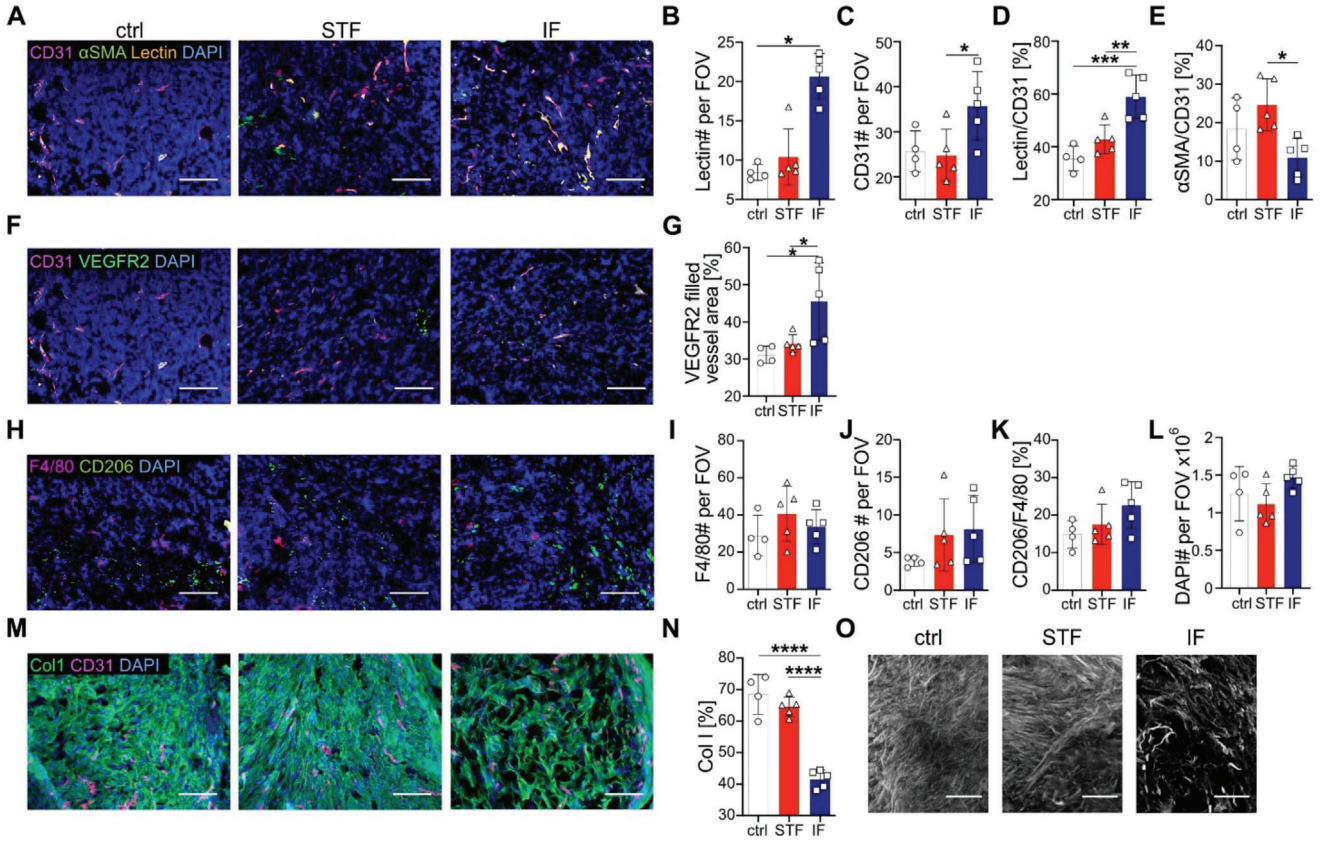

Figure 2. Intermittent fasting alters the composition of the tumor microenvironment. A) Fluorescent microscopy images showing CD31$^+$ blood vessels, lectin$^+$ perfused functional blood vessels, and αSMA$^+$ pericyte covered blood vessels. Nuclei are counterstained using DAPI. B–E) Quantifying tumor vasculature features upon fasting shows a significant increase in vessel perfusion upon IF. F) Fluorescence microscopy images showing DAPI$^+$ cell nuclei, blood CD31$^+$ vessels (CD31), VEGFR2$^+$ angiogenic vessels. G) Quantifying the fraction of VEGFR2$^+$ blood vessels indicate an increase in angiogenesis upon IF. H) Fluorescence microscopy images showing DAPI$^+$ cell nuclei, F4/80$^+$ macrophages, and CD206$^+$ macrophages upon fasting. I–L) Quantification of macrophage and cell density in tumors upon fasting. M) Fluorescence microscopy images showing collagen I (Col I) deposition, blood vessels, and cell nuclei upon fasting. N) Quantification of microscopy images shows a significant decrease in collagen deposition upon IF. All scale bars indicate 25 µm. O) Two-photon laser scanning microscopy images showing collagen density. Scale bars indicate 100 µm. All values represent means ± SD ($n = 4$ ctrl, $n = 5$ STF, IF). One-way ANOVA and Tukey's multiple comparisons test were used for statistical analysis. ****$P < 0.0001$, ***$P < 0.001$, **$P < 0.01$, *$P < 0.05$, ns = not significant ($P > 0.05$).

Thus, intermittent fasting reduces tumor growth and improves liposome delivery in subcutaneous hepatoma tumors.

2.2. IF Primes the TME of Subcutaneous Tumors in Favor of Tumor-Targeted Delivery

Encouraged by the notion that IF improves liposome delivery, we next investigated the impact of IF and STF on the composition of tumor microenvironment (TME) that may impact the transport and uptake of liposomes. One central aspect of drug delivery is tumor vascularization and perfusion.[25] Hence, we analyzed changes in vessel formation and angiogenic factors via immunofluorescence staining (**Figure 2**A–E). We found a significantly higher count of functional vessels as indicated by lectin perfusion (Figure 2B) as well as total CD31$^+$ blood vessels upon IF (Figure 2C). Also, the percentage of perfused vessels (Figure 2D) and the number of angiogenic VEGFR2-expressing blood vessels (Figure 2F,G) were increased. Conversely, the percentage of pericyte-coverage on blood vessels, an essential part of the vascular endothelial barrier, was found to be reduced (Figure 2E). Taken together, IF leads to increased tumoral vascularization and perfusion, which likely accounts for the improved tumor-targeted delivery of liposomes.

The presence of tumor-associated macrophages (TAMs) also influences liposome uptake,[13] and as of yet, the impact of fasting on TAMs has not been studied.[26] We therefore examined the accumulation of macrophages under the different fasting conditions (Figure 2H–K). The number of F4/80$^+$ macrophages, i.e., all macrophages, did not differ between the two fasting groups (Figure 2I). A slight increase in CD206$^+$ macrophages, i.e., M2-like macrophages, was observed for STF and IF (Figure 2J). The fraction of M2-like macrophages was higher upon IF but this was not statistically significant (Figure 2K). In addition, the total cell density (i.e., all DAPI$^+$ nuclei) was also not affected by fasting (Figure 2L).

Another main component of TME is the extracellular matrix (ECM), which acts as a barrier in the penetration of drugs and

drug delivery systems into tumor tissue.[14] The abundance of collagen 1 (Col I), a main structural part of the ECM, was studied upon fasting (Figure 2M–O). In the IF group, there was a significantly lower abundance of Col I, with an area fraction of 37.98%, compared to control (59,86%; $P = 0.0001$) and STF (60.64%; $P = 0.0001$). Hence, IF impacts TME by increasing functional vascularization and decreasing collagen density, together promoting tumor-directed liposome delivery.

2.3. Fasting Increases Liposome Tumor Cell Uptake via Caveolae-Mediated Endocytosis

We next examined the impact of fasting on liposome uptake at the cellular level. To this end, we studied the effect of the adenylyl cyclase inhibitor forskolin on Hep-55.1C and Hepa1.6 cells (**Figure 3**A). Forskolin stimulates lipid and carbohydrate metabolism by activating intracellular cAMP pathways, as does fasting in vivo.[27] In order to differentiate the mechanism by which liposome cancer cell uptake is performed, we employed different endocytosis inhibitors. Nystatin, which sequesters cholesterol and other lipids from cell membranes thereby inhibiting caveolae-mediated endocytosis,[28] was found to be the most potent inhibitor of liposome uptake by hepatocellular carcinoma cells (Figure suppinfo1, Supporting Information). Nystatin was subsequently combined with forskolin to study liposome uptake upon fasting mimicry. This was examined by flow cytometry and/or immunofluorescence microscopy. Forskolin stimulation produced a significant increase in liposome uptake in Hep-55.1C and Hepa1.6 cells (Figure 3B,C,F,H,J,L). Nystatin cotreatment completely abolished the uptake-enhancing effects of forskolin in both cell lines (Figure 3D,E,G,I,K,M). Together, these findings show that liposome internalization by hepatoma cells is increased upon fasting and that this effect is mediated by caveolar endocytosis.

2.4. IF Attenuates Intrahepatic Tumor Growth and Enhances Liposome Delivery

Subcutaneous and orthotopic tumors can differ substantially in terms of tumor development, vascularization and TME composition,[29] which may impact the effect that fasting has on tumor-directed delivery and accumulation. Liver cancer in general exhibits a high drug clearance rate and unfavorable drug distribution using conventional chemotherapy, making alternatives employing drug delivery systems conceptually appealing.[30] To evaluate whether fasting also influences orthotopic hepatocellular carcinomas, we surgically inoculated Hep-55.1C cells into the left lateral liver lobe of mice. Since we did not find significant differences between the control and the STF group in the subcutaneous model in terms of liposome accumulation and TME composition, mice were then either fed ad libitum in the control group or intermittently fasted for three weeks in the IF model. To support postsurgical recovery, IF was not started until day 3 after tumor inoculation. Similar to the subcutaneous model (Figure 1C), mice in the IF group initially lost a significant amount of weight but recovered to match the weights of animals in the control group from day 9 onwards (**Figure 4**A). Weekly MRI scans showed reduced intrahepatic tumor growth upon IF (Figure 4B,C). Due to the strong intrahepatic tumor growth under ad libitum conditions, we observed a pronounced displacement of the liver, which was macroscopically visible in the upper right abdominal quadrant (Figure 4D). Importantly, no such displacement was observed in the IF group (Figure 4D). In line with this, we saw a lower tumor-to-body weight and tumor-to-liver weight ratio upon IF (Figure 4E–H). These results confirm that hepatoma tumor growth is reduced upon IF.

To investigate the impact of IF on the tumor accumulation of Cy7-labeled liposomes in the intrahepatic model, μCT-FLT was again performed up until 72 h p.i. (Figure 4I–K). To localize intrahepatic tumors more accurately, the CT contrast agent Imeron400 was also injected. At all-time points p.i., the tumor accumulation of liposomes was much higher for IF than for controls (Figure 4J). The IF group had 2.9-fold increase 72 h p.i. compared to the control group (control: 14.41%IF/g, IF 41.45%ID/g; $P = 0.18$). Liposome accumulation in the healthy liver tissue was comparable in both groups (Figure 4K). Semi-quantitative ex vivo FRI analysis of resected tissues confirmed the in vivo biodistribution patterns (Figure 4L–N). Increased tumor uptake was furthermore validated by assessing the percentage of PEG^+-stained area, which was significantly increased (Figure 4O). Altogether, IF attenuates intrahepatic tumor growth and enhances liver tumor-targeted liposome delivery.

2.5. The Intrahepatic Tumor Microenvironment is Altered upon IF

To strengthen the above findings, we next examined the intrahepatic TME upon fasting. As in the subcutaneous tumor model, IF beneficially primed hepatomas towards improved liposome delivery, as evidenced by increased vessel density and enhanced vascular perfusion (**Figure 5**A–E). Also, VEGFR2 expression on blood vessels, as a marker of angiogenesis, was significantly increased (Figure 5F,G). The percentage of pericyte-covered blood vessels, as part of the endothelial barrier, was significantly reduced (Figure 5E). IF did not impact the number and polarization of infiltrating TAMs, determined by the fact that the counts of $F4/80^+$ macrophages and of $CD206^+$ macrophages were not significantly different (Figure 5H–K). Fasting also did not impact the overall intrahepatic cellular density, as the count of $DAPI^+$ nuclei did not differ between both groups (Figure 5L). Regarding ECM deposition, we visualized and quantified collagen I (Col I), observing a significant decrease in collagen density upon IF as compared to the control group (Figure 5M–O). In summary, the results obtained in the intrahepatic model are consistent with those of the subcutaneous model, and they together support the concept that IF remodels the TME and enhances tumor-targeted liposome delivery.

2.6. IF Improves Therapeutic Outcome Following Doxil Treatment and Reduces Chemotherapy-Associated Side Effects

We further examined if IF influences treatment response in addition to its intrinsic impact on tumor growth. We studied the

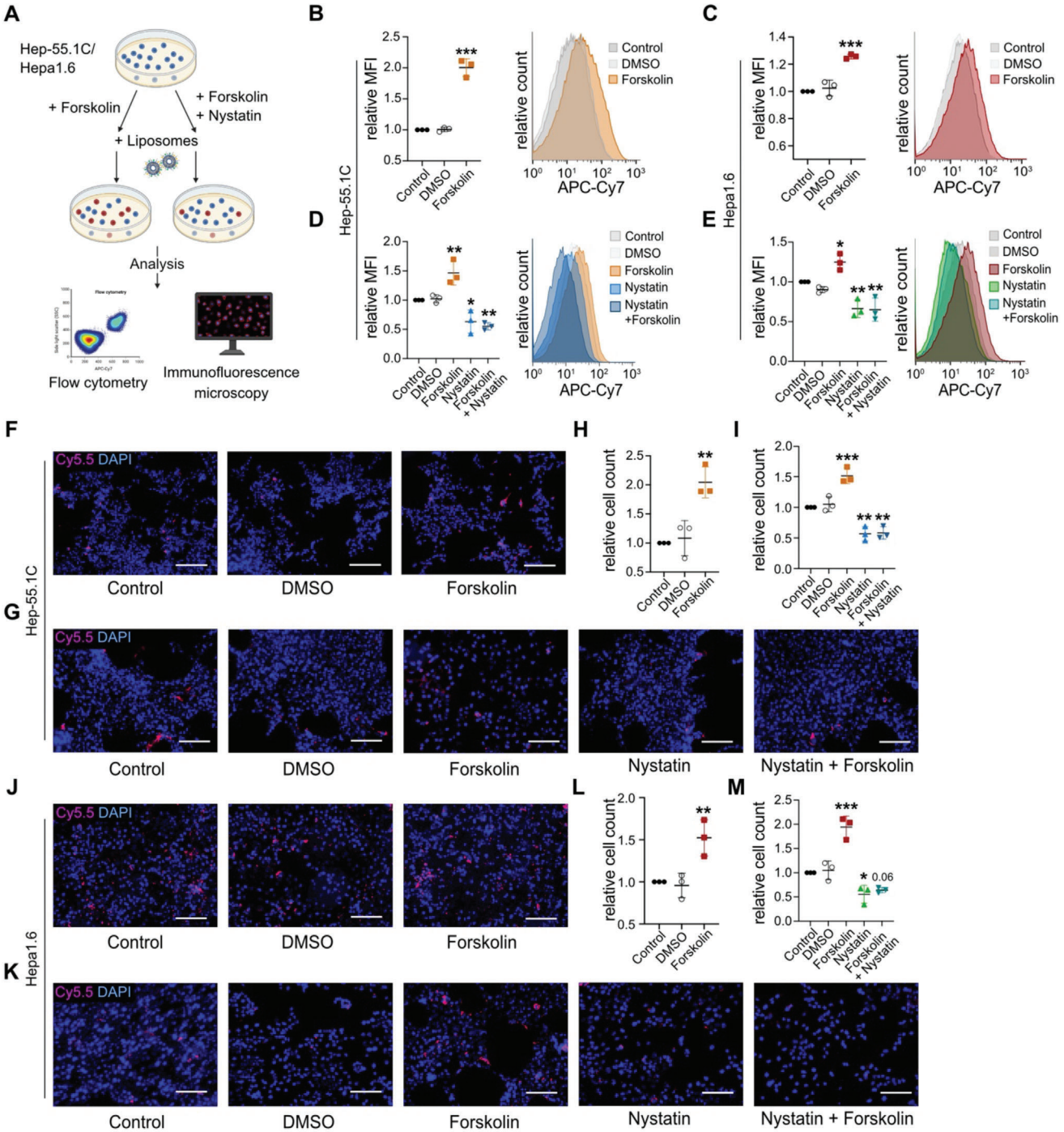

Figure 3. Fasting stimulates liposome cell uptake via caveolae-mediated endocytosis. A) Schematic representation of the experiment performed with the hepatoma cancer cell lines Hepa1.6 and Hep-55.1C. Fasting was mimicked using forskolin, and nystatin inhibited its effect on liposome uptake. The uptake of fluorescently labeled liposomes was analyzed via flow cytometry and fluorescence microscopy. B,C) Flow cytometry analysis and quantification of the uptake of Cy5.5-labeled liposomes upon forskolin treatment in Hep-55.1C (B) and Hepa1.6 (C) cells, showing significantly increased liposome uptake upon forskolin-based fasting mimicry. D,E) Forskolin-enhanced liposome uptake is significantly reduced by the caveolae-mediated endocytosis inhibitor nystatin in Hep-55.1C (D) and Hepa1.6 (E) cells. F–I) Representative fluorescence microscopy images (F, G) and quantification (H, I) of Cy5.5-liposome uptake upon forskolin and forskolin in costimulation with nystatin in Hep-55.1C. J–M) Representative fluorescence microscopy (J, K) images and quantification (L, M) of Cy5.5-liposome uptake by Hepa1.6 cells upon treatment with forskolin and/or nystatin and their uptake of liposomes. All values represent means ± SD. One-way ANOVA and Tukey's multiple comparisons test were used for statistical analysis. ****$P < 0.0001$, ***$P < 0.001$, **$P < 0.01$, *$P < 0.05$, ns = not significant ($P > 0.05$). Scale bars indicate 25 µm. The figure was created with Biorender.

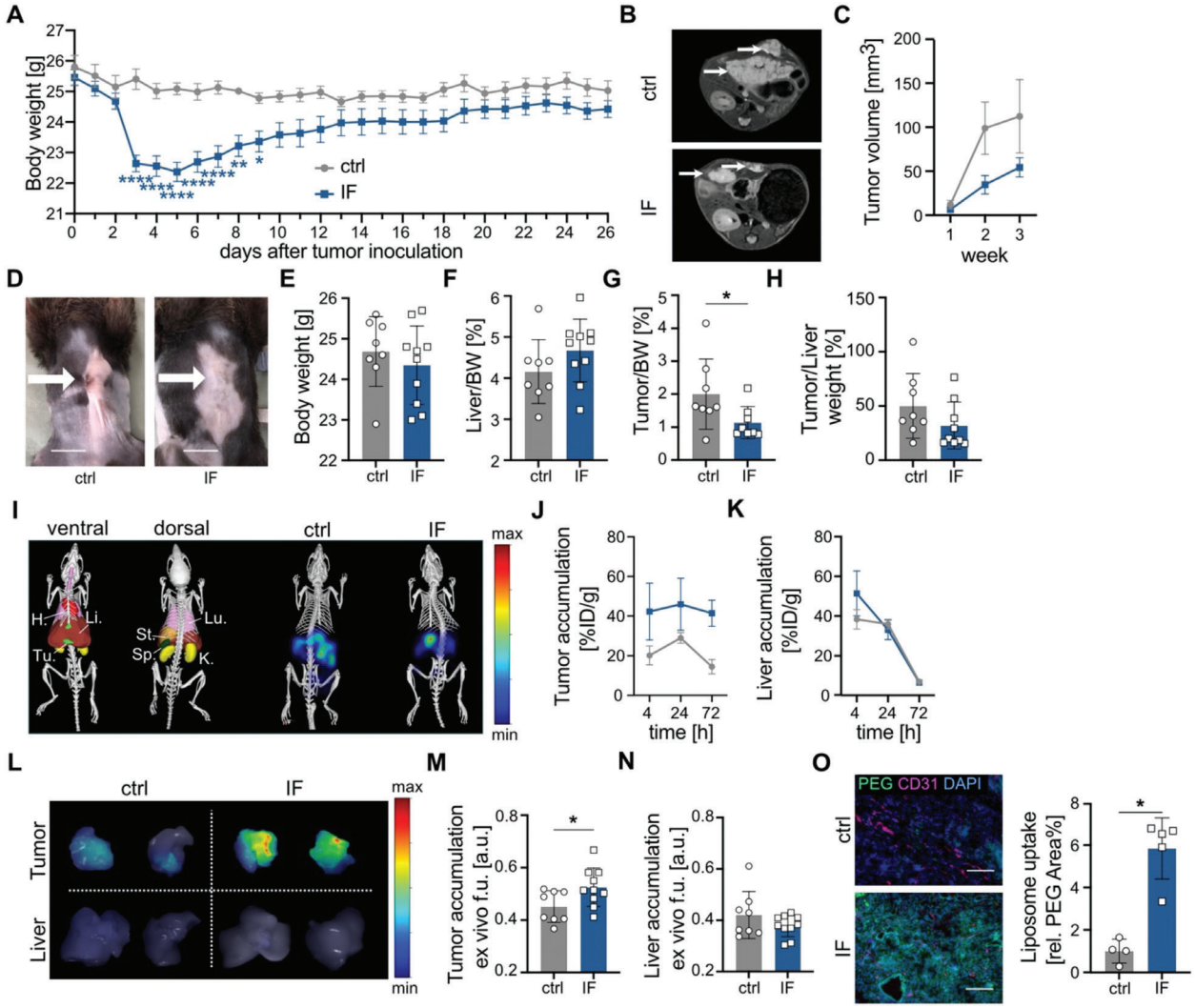

Figure 4. Intermittent fasting increases liposome accumulation in intrahepatic tumors. A) Mice were inoculated intrahepatically with Hep-55.1C cells. The third night after tumor inoculation, overnight IF was initiated. Body weight was monitored daily. Values represent mean ± SEM ($n = 8$ ctrl, $n = 10$ IF). Two-way ANOVA and Šidák's multiple comparisons test were used for statistical analysis. B,C) Representative MRI scans (B) and quantification (C) of the effect of IF on intrahepatic tumor growth. Tumors are indicated with white arrows. Values represent mean ± SEM ($n = 8$ ctrl, $n = 10$ IF). Two-way ANOVA and Šidák's multiple comparisons test were used. D) Representative images of the torso of mice fed either ad libitum (ctrl) or subjected to IF show that increased tumor growth could be observed externally in ctrl mice, whereas in IF mice, not. Scale bar indicates 1 cm. E–H) Upon sacrifice, the whole-body, liver, and tumor weights were determined and compared. Values represent mean ± SD ($n = 8$ ctrl, $n = 10$ IF). An unpaired *t*-test was performed for body weight and liver/body weight ratio. Mann–Whitney test was performed for tumor/body weight ratio and tumor/liver weight ratio due to non-normal distribution. I) Liposome distribution and tumor accumulation were assessed via μCT-FLT. 3D reconstruction of μCT-based organ segmentation is shown on the left. Lu. = lungs, Li. = liver, St. = stomach, Sp. = spleen, K. = kidneys, Tu. = tumor. Representative scans are shown for 72 h post i.v. injection of Cy7-labeled liposomes. J,K) Quantification of liposome biodistribution shows higher tumor accumulation (%ID/g) upon IF, while accumulation in the liver is similar between control and IF-fasted mice. Values represent mean ± SEM ($n = 4$ ctrl., $n = 5$ IF). Two-way ANOVA and Šidák's multiple comparisons test were used for statistical analysis. L) Representative *ex vivo* 2D FRI scans of livers and tumors. M,N) Quantification of ex vivo 2D FRI scans confirmed increased liposome accumulation in tumors and livers upon IF. Values represent mean ± SD ($n = 8$ ctrl, $n = 10$ IF). An unpaired *t*-test was performed. O,P) Fluorescence microscopy images exemplifying liposome distribution (anti-PEG staining), cell nuclei (DAPI), and blood vessels (CD31) in intrahepatic tumors (O), showing that IF increases liposome accumulation and lowers liver localization. Scale bars indicate 25 μm. Values represent mean ± SD ($n = 4$ ctrl, $n = 5$ IF). Unpaired *t*-tests were performed for statistical analysis. $^*P < 0.05$, ns = not significant ($P > 0.05$).

effect of IF on drug delivery and efficacy using free and liposomal doxorubicin in the subcutaneous Hep-55.1C tumor model. Animals were divided into two groups: one group was subjected to intermittent fasting, and the other group was provided unrestricted access to food and water. Each group was further divided into subgroups receiving either a control saline solution (NaCl), free doxorubicin (Dox), or liposomal doxorubicin (Doxil) twice a week for three weeks (**Figure 6**A,B).

To examine the impact of combining IF with chemotherapy on the well-being of the mice, we closely monitored their

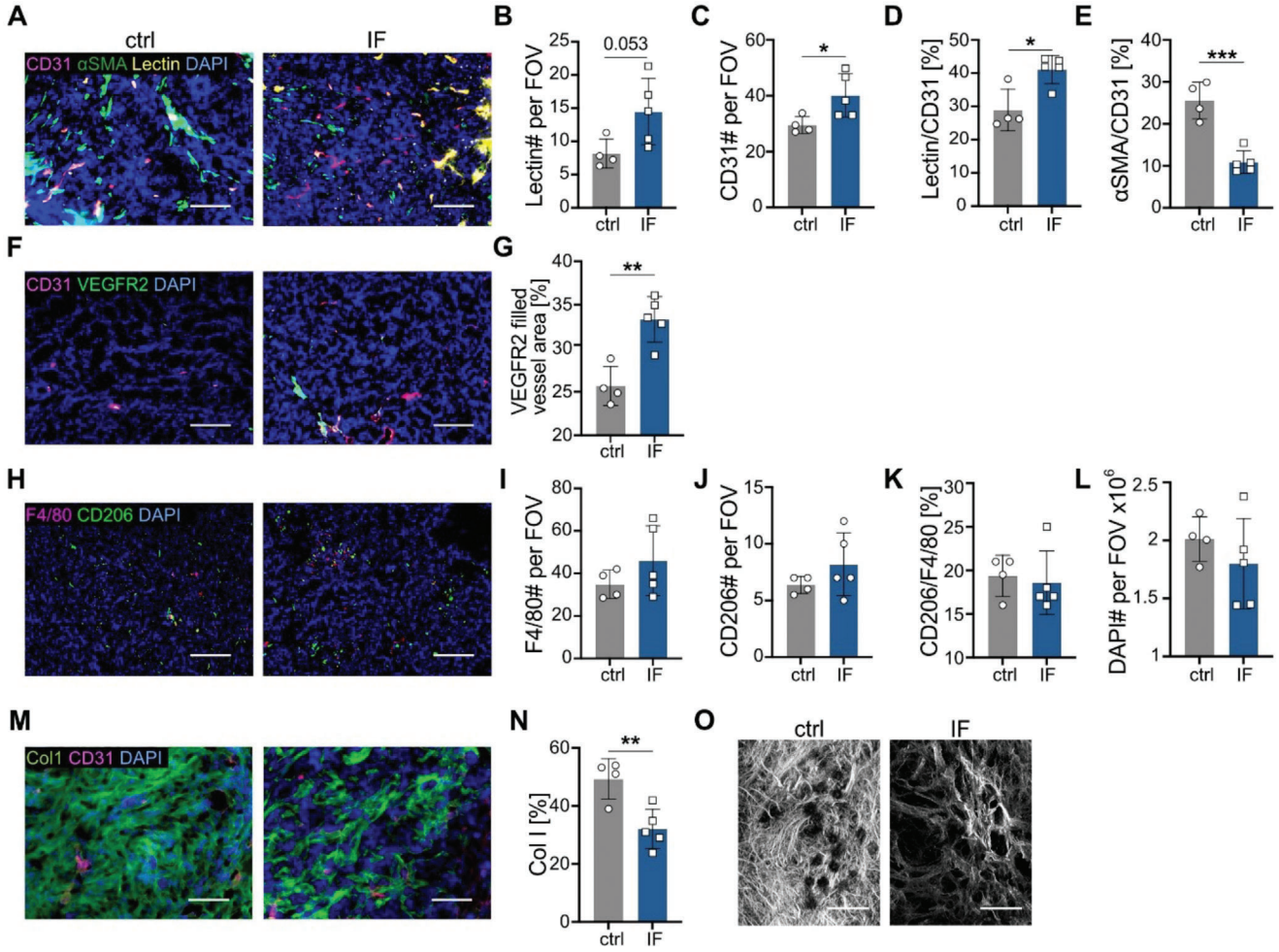

Figure 5. Intermittent fasting alters the intrahepatic tumor microenvironment. A) Fluorescent microscopy images showing CD31$^+$ blood vessels, lectin$^+$ perfused blood vessels, and αSMA$^+$ pericytes. Nuclei are counterstained using DAPI. B–E) Quantification shows an increase in vessel density and perfusion and a decrease in pericyte coverage upon IF. F,G) Fluorescence microscopy analysis (F) and quantification (G) of VEGF receptor 2 (VEGFR2) expression in CD31$^+$ blood vessels, showing a significant increase in the fraction of angiogenic blood vessels upon IF. H) Fluorescence microscopy images showing DAPI$^+$ cell nuclei, F4/80$^+$ macrophages, and CD206$^+$ M2-like macrophages. I–L) Quantification of macrophage and cell density shows no significant differences upon IF. M,N) Fluorescence microscopy images (M) and quantification (N) of collagen I (Col I) expression showed significantly less collagen deposition in tumors upon IF. All scale bars indicate 25 µm. O) Two-photon laser scanning microscopy images showing collagen density. The scale bars indicate 100 µm. Values represent mean ± SD ($n = 4$ ctrl, $n = 5$ IF). An unpaired t-test was used for statistical analysis. ***$P < 0.001$, **$P < 0.01$, *$P < 0.05$, ns = not significant ($P > 0.05$). Scale bars indicate 25 µm.

body weight (Figure 6C). Here, the previously observed recovery of weight loss in mice during IF was also found in the chemotherapy groups. After an initial period of weight loss, the body weight of mice treated with Dox remained stable. Conversely, IF mice treated with Doxil consistently increased in body weight throughout the duration of treatment. By the end of the treatment, no significant difference in the average body weight between the fasting control mice and the Doxil-treated mice was observed. This suggests that employing IF could serve as a promising strategy to mitigate detrimental health consequences associated with weight loss in cancer (nano)therapy (Figure 6D).

Consistent with previous results, assessing the effect of dietary restriction on tumor progression confirmed that IF attenuates tumor growth (Figure 6E), a trend that applied to all therapeutic conditions. Additionally, IF in combination with Doxil treatment not only had a significant impact on tumor progression, but exhibited a further decrease in overall tumor volume compared to treatment with Doxil alone (Figure 6F). Moreover, IF significantly lowered the final tumor volume compared to all other therapy groups.

To investigate the impact of fasting on Doxil efficacy at the tissue and cellular level, we stained ex vivo tumor sections for DAPI (cell nuclei) and TUNEL (apoptotic cell death), as presented in the immunofluorescence images in Figure 6G. While the number and density of nuclei in tumor sections remained unchanged between IF and non-fasting treatment groups (Figure 6H), administering Doxil in combination with IF significantly increased cell death (Figure 6I), as evidenced by the significantly greater number of cells positive for TUNEL staining.

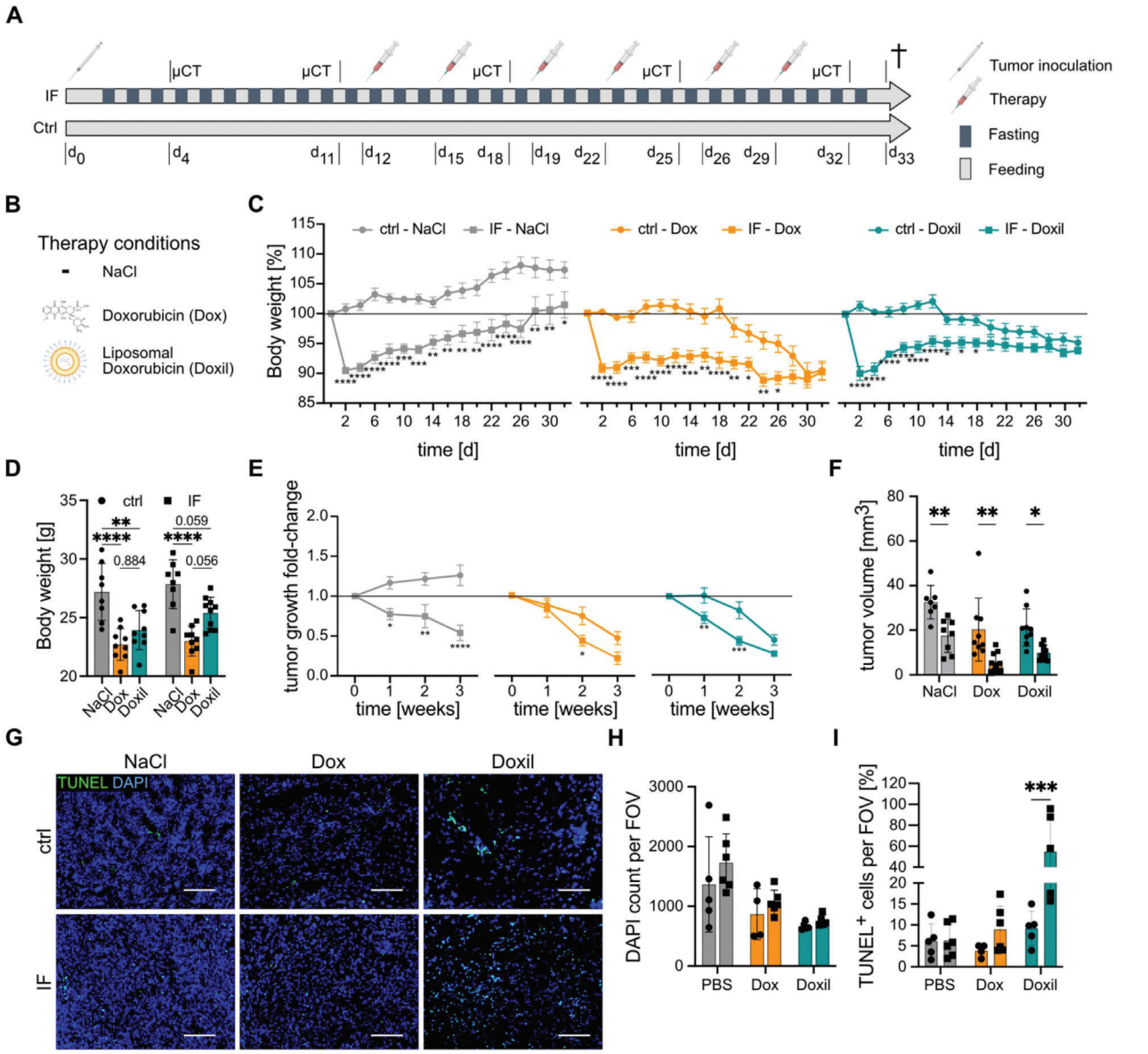

Figure 6. Intermittent fasting increases Doxil treatment efficacy and intratumoral cell death. A) Schematic timeline of intermittent fasting conditions concomitant to therapy. B) Overview of the therapy conditions applied. C) The body weight was measured every morning. IF was initiated two days after tumor inoculation. Therapy conditions were applied 12 d after tumor inoculation, twice per week over three weeks. Values represent mean ± SEM (ctrl NaCl $n = 8$, ctrl Dox $n = 9$, ctrl Doxil $n = 9$, IF NaCl $n = 8$, IF Dox $n = 9$, IF Doxil $n = 10$ mice). D) Quantification of the body weight differences due to IF concomitant to chemotherapy upon sacrifice. Values represent mean ± SD (ctrl NaCl $n = 8$, ctrl Dox $n = 9$, ctrl Doxil $n = 9$, IF NaCl $n = 8$, IF Dox $n = 9$, IF Doxil $n = 10$ mice). E) Weekly μCT scans showed a reduction in tumor growth upon IF in each therapy condition. Values represent mean ± SEM (ctrl NaCl $n = 8$, ctrl Dox $n = 9$, ctrl Doxil $n = 9$, IF NaCl $n = 8$, IF Dox $n = 9$, IF Doxil $n = 10$ mice). F) End tumor volumes measured in the last μCT scan before sacrifice showed significant reductions in tumor volumes upon IF in each therapy condition. Values represent mean ± SEM (ctrl NaCl $n = 8$, ctrl Dox $n = 9$, ctrl Doxil $n = 9$, IF NaCl $n = 8$, IF Dox $n = 9$, IF Doxil $n = 10$ mice). G) Representative fluorescence microscopy images showing the induction of intratumoral apoptosis (TUNEL) by the therapy conditions in cell nuclei (DAPI). H,I) Quantification of cell density and percentage of TNUEL+ cell in tumors upon IF concomitant to therapy conditions. Values represent mean ± SD (ctrl NaCl $n = 5$, ctrl Dox $n = 4$, ctrl Doxil $n = 5$, IF NaCl $n = 6$, IF Dox $n = 6$, IF Doxil $n = 5$ mice). The scale bar indicates 25 μm. All statistical analyses are based on Two-way ANOVA and Šidák's multiple comparisons test. ****$P < 0.0001$, ***$P < 0.001$, **$P < 0.01$, *$P < 0.05$, ns = not significant ($P > 0.05$).

3. Discussion

In this study, we demonstrate that intermittent fasting (IF) attenuates tumor growth, alters the tumor microenvironment (TME), improves liposome cell uptake and enhances tumor-targeted drug delivery, altogether improving nanochemotherapy treatment outcome. Short-term fasting was applied in a subcutaneous HCC model, while intermittent fasting was evaluated in both subcutaneous and intrahepatic HCC models. Chemotherapy efficacy was only studied in the subcutaneous IF model, since results

obtained in the subcutaneous model did not differ significantly from the intrahepatic model.

In both allogeneic models, we found reduced tumor growth upon IF, but not STF in the subcutaneous model. This is in line with previous studies that have shown that IF can suppress tumor progression.[23,31–33] An important contributing factor is a high energy and nutrient demand of tumor cells to achieve continuous cell proliferation, which cannot be maintained under fasting conditions.[31] Nutritional supply and intratumoral metabolism are also controlled to a greater extend by the extracellular matrix (ECM).[34] Upon IF, we saw a significant reduction in collagen abundance (Figures 2M–O and 4M–O), which may also contribute to reduced tumor growth, since a lower collagen density results in lowered activation of certain growth-promoting factors, such as TGF-β and EGFR.[35] The finding of increased angiogenesis stands in contrast to reduced tumor growth upon IF. However, this could be attributed to compensatory mechanisms induced by nutrient-deprived tumor cells to maintain nutrient supply and might not have a strong enough net effect to counteract growth reduction. Notably, IF should not be considered as a stand-alone therapeutic modality to suppress tumor progression in a clinical setting, but rather as a neo/adjuvant treatment option to increase the efficacy and tolerability of systemic drug therapy.[9]

Upon IF, we achieved a fivefold increase in tumor liposome uptake in the subcutaneous model, and a 2.5-fold increase in the intrahepatic model (Figures 1F–I and 4I–P). These results, in line with previous reports showing increased efficacy upon fasting, make IF an attractive approach to combine with nanomedicine therapy. At the tumor cell level, a contributing factor to increased liposome accumulation appears to be increased liposome internalization, given that forskolin treatment-mimicking fasting prominently promoted Hep-55.1C and Hepa1.6 hepatoma cell uptake (Figure 3B,C,F–I).[27] Concurrent inhibition with nystatin decreased uptake to levels below baseline (Figure 3D,E,J–M), implicating caveolae-mediated endocytosis as the primary mechanism of fasting-induced uptake in vitro. At the tumor tissue level, we found that IF induced angiogenesis and reduced ECM deposition. It has been shown that during wound healing fasting facilitates neovascularization through upregulating proangiogenic genes.[36] This aligns with our findings that vascular density, perfusion, and VEGFR2 expression were significantly increased upon IF (Figures 2F–L and 4F–L), ensuring that drugs and drug delivery systems enter and access tumors more efficiently. We furthermore found that the percentage of pericyte-covered blood vessels decreased (Figures 2J and 4J), which may result in increased permeability and enhanced drug delivery system extravasation.[37,38] Considering that a dense ECM typically acts as a barrier for nanoparticle penetration,[14] we next studied collagen density in tumors and observed a significant reduction (Figures 2M,N and 4M,N). This may allow liposomes and other nanomedicine formulations to penetrate deeper and distribute more homogenously. Lastly, we studied tumor-associated macrophages (TAMs), which can act as a slow release reservoir for nanomedicines.[13] IF did not change TAM infiltration and polarization (Figures 2A–D and 4A–D), thus the retention component of nanomedicine tumor accumulation appears to be unaffected.

Since IF showed enhanced liposome accumulation, we also studied its impact on treatment response. We observed a significant reduction in tumor volume following treatment with free Dox and Doxil in IF mice. Notably, during IF, we observed enhanced vascularization and reduced collagen deposition, which likely promoted the tumor accumulation of both chemotherapeutic drugs. Combining IF with Doxil treatment resulted in a significantly greater reduction in tumor growth as compared to IF plus free Dox. This finding was corroborated by an increased rate of cell death in tumors following Doxil treatment in IF mice, suggesting a synergistic effect of combined nanotherapy and intermittent fasting.[4] Taken together, these results support the hypothesis that the modulation of angiogenesis and collagen induced by intermittent fasting constitutes a key enabling factor in the overall enhancement of nanochemotherapy efficacy.[39,40]

Earlier reports indicate that caloric restriction, including intermittent fasting, has a mitigating effect on chemotherapy-related side effects, positively impacting patient or subject well-being during treatment.[41,42] Consistent with these reports, our study demonstrates a positive impact of IF during treatment, as mice exhibited rapid recovery and improved body weight maintenance throughout the duration of treatment. This improvement in weight regulation during concomitant IF and Doxil therapy may result from the reduced tumor growth combined with the improved therapy response. These findings emphasize the potential synergistic benefits of combining IF with nanotherapies, presenting an opportunity to improve cancer therapy in terms of their efficacy as well as tolerability.

Our findings suggest that IF is a promising neo/adjuvant addition to treatment to help improve nanomedicine delivery and potentiate therapy outcome. Strategies to improve tumor targeting that do not rely on stimuli-responsive materials and targeting ligands have remained relatively elusive.[17] Our TME priming results and efficacy enhancement suggest that IF may be a low-cost, broadly applicable, and easily accessible strategy to boost drug delivery to HCC lesions. This is independent of whether they are passively or actively targeted, and/or whether they rely on local triggering of, e.g., temperature-sensitive liposomal drugs to enhance drug release.[21] Importantly, the observed IF-induced increases in vascularization and tumor perfusion, as well as the reduced collagen density contribute to the improvement of HCC drug targeting and therapy. Altogether, we conclude that concomitant fasting primes tumors for better drug delivery and nanotherapy efficacy.

4. Experimental Section

Animals: All mice were treated in accordance with the criteria of the German administrative panels on laboratory animal care as outlined in the "Guide for the Care and Use of Laboratory Animals" prepared by the National Academy of Sciences and published by the National Institutes of Health (NIH publication 86-23 revised 1985). All animal experiments were approved by the appropriate German authorities (LANUV. North Rhine-Westphalia).

Seven-week-old C57BL/6J male mice were purchased from Janvier Labs (Le Genest-Saint-Isle, France) and housed in a specific pathogen-free environment (maximum four per cage), under standard 12-h light/12-h dark cycles and at a temperature of 21–23 °C with a relative humidity of 35–65%. After 7 d of acclimation, mice were initiated on tumor injection under anesthesia. The tumor protocol was adapted from Wirtz et al. 2022.[43] The subcutaneous tumor was placed in the left flank upon hair removal. Fasting began the following day. Due to surgery, mice with an intrahepatic

tumor were given two days to recover before fasting therapy was applied. Mice were randomly assigned to the respective groups, with 8–11 mice per group. At the time of sacrifice, mice were anesthetized using isoflurane, followed by cervical dislocation and organ removal.

Fasting Therapies: The protocol for fasting therapies was adapted from Hatting et al. 2017,[22] with slight modifications. Mice were treated with two fasting therapies throughout the studies. On the evening of 0 d of therapy (DOT), the intermittent fasting (IF) group was initiated to fast for 12 h every night during the active phase. In the evening, after 20 DOT, the short-time fasting (STF) group was fasted once. The control group was treated ad libitum. In all cases, mice have changed between two cages alternatively. In the fasting cage, no food was added, but drinking water was always supplied. In order to reduce autofluorescence, especially in the gastrointestinal region, and thus improve fluorescence imaging, the animals were fed a specific chlorophyll-free diet (Sniff, E15051, Soest, Germany). The body weight and condition of the animals were observed daily.

Chemotherapy: Mice were divided into a control and IF group. Eleven days post-tumor inoculation, chemotherapy was administered i.v. twice a week over a three-week period. Chemotherapy consisted of either a control saline solution (NaCl), free doxorubicin (Dox), or liposomal doxorubicin (Doxil). A dose of 5 mg kg^{-1} of doxorubicin was administered per injection. All injections were performed under anesthesia.

Imaging Protocol: Tumor growth was evaluated in weekly scans using either μCT (subcutaneous tumor) or a 7-T MRI scanner (BioSpec 70/20 USR; Bruker, Ettlingen, Germany) with a transceiver mouse volume coil. Mice were imaged according to a representative MRI protocol:[1] localization of liver by transversal T1-RARE sequences,[2] T2-weighted spin echo liver MRI with respiratory gating. Analysis of MRI scans was performed with the ParaVision 6 software (Bruker, Billerica, USA).

For the dehairing of the abdomen and imaging procedures, mice were anesthetized using isoflurane (Forene, Abbott, Wiesbaden, Germany) in oxygen-enriched air using a vaporizer. Eyes were protected with bepanthen eye ointment (Bayer Vital GmbH, Germany) from desiccation. For intravenous injection, a sterile catheter was placed into the lateral tail vein of the mouse. The catheter was prepared beforehand by connecting a 30 G cannula (B.Braun, Melsungen, Germany) to a polyethylene tube with an inner diameter of 0.28 mm and outer diameter of 0.61 mm, and a wall thickness of 0.165 mm (Hartenstein, Würzburg, Germany). Mice were i.v. injected with Cy7-labeled liposomes (2 nmol dye content; in 50 μL 0.9% NaCl sterile solution) for quantifying the biodistribution and tumor accumulation. Each mouse was scanned before injection and 0.25, 4, 24, 48, and 72 h post-injection (subcutaneous model). In the intrahepatic model, Imeron 400 MCT (Bracco Imaging GmbH, Germany) was i.v. injected 4, 24, and 72 h post-injection with a dose of 5 mL kg^{-1} BW. The mice were placed in an animal cassette which holds the animal tightly between two acrylic glass plates (3 mm thickness). The μCT-FLT device (U-CT OI, MILabs B.V., Utrecht, The Netherlands) used in this study, consists of a cooled CCD camera (−65 °C) in combination with a high-resolution μCT. First, the animal holder was automatically moved to the front of the device between FLT laser and cooled CCD camera. For scanning, a laser with 730 nm wavelength and an emission filter (775 nm + 25 nm) were used to acquire excitation and emission images of ≈130 laser points. After acquiring the FLT scan, the animal holder was automatically moved to the CT to acquire a total body μCT scan. In a full-rotation in step-and-shoot mode, 480 projections (1944 × 1536 pixels) were acquired with an X-ray tube voltage of 55 kV, power 0.17 mA, exposure time of 75 ms, and low-dose (≈0.1 Gy/whole body scan). To cover the entire animal, two subscans were acquired. After μCT-FLT imaging, organs were excised and scanned by 2D reflectance imaging at 750 nm excitation wavelength (FMT 4000, PerkinElmer, Waltham, MA, USA). After the last CT-FLT scan, the animals were sacrificed, and organs were excised for ex vivo evaluation.

Two-Photon Laser Scanning Microscopy: Unstained 100 μm thick cryosections were imaged via two-photon laser scanning microscopy (TPLSM) using a Leica Stellaris 8 Dive Falcon multiphoton microscope equipped with a 25x/1.00 HC IRAPO water-immersed objective (Leica Microsystems, Germany) to assess collagen content. To visualize second harmonic generation of collagen, emission was detected using the HyD NDD2 hybrid-detector tuned to an emission range of 390–420 nm, following excitation by a pulsed InSight X3 dual laser (Spectra Physics, United States) tuned to 800 nm. A series of subsequent 1024 × 1024 pixel *xy*-stacks were imaged in 1.5 μm z-steps and constructed into a maximal projection. 3D reconstruction and image processing was conducted using Leica LAS X 3D (Leica Microsystems, Germany) and Imaris (Bitplane, Switzerland) software.

Image Analysis: All acquired 3D μCT images were reconstructed at an isotropic voxel size of 80 μm using a Feldkamp type algorithm (filtered backprojection). 3D organ segmentations were generated based on the μCT data using interactive segmentation operations (Imalytics Preclinical, Gremse-IT GmbH, Aachen, Germany). Segmentations of heart, lungs, liver, spleen, kidneys, and tumor were generated for all mice at all points in time. For calibration, the fluorescence signal in the entire animal in the FLT scans directly after injection was used to generate a scale factor and concentrations (%ID g^{-1}) were computed by assuming density of 1 g cm^{-3} for each voxel.[44]

Liposomes: Liposomes were prepared by ethanol dilution.[45,46] Briefly, 0.246 × 10^{-3} M DPPC (Lipoid, Germany), 0.133 × 10^{-3} M Cholesterol (SigmaAldrich, Germany), and 0.02 × 10^{-3} M PEG (2000)-DSPE (Lipoid, Germany) were diluted in 10 mL Chloroform (AppliChem, Germany) together with 0.75 × 10^{-9} M Cy7-DPSE or Cy5.5-DPSE (AvantiPolarLipids, United States). Under a low vacuum at 70 °C, the solution was dried for 1 h in the rotary evaporator. Then, 10 mL PBS was added and stirred without vacuum at 70 °C. To extrude, liposomes were filtered twice at 200 nm, three times 100 nm (Liposofast LF-50; Avestin, Germany), and sterilized with a 0.2 μm syringe filter. Characterization was performed with DLS (Zetasizer Nano; Malvern, UK) and a plate reader (M200pro; Tecan, Switzerland) for fluorescence.

Histology and Immunohistochemistry: After collection, tissue specimens were immediately embedded in Tissue-Tek. Tissues were cut into 8 μm-thick sections by using a cryotome (CM3050S, Leica Biosystems, Germany). Slides were air-dried for 30 min at RT. Stainings for vessel formation, macrophage accumulation, and Collagen1 abundance were performed according to Biancacci et al. 2022.[44] VEGFR2 and PEG stainings were performed with the respective primary and secondary antibodies. Briefly, the tissue slides were washed three times 1 min in phosphate-buffered saline (PBS) and fixed for 5 min in 80% Methanol (Honeywell Research Chemicals, 10 163 383), followed by 2 min in ice-cold Acetone (Honeywell Research Chemicals, RD32201). Then, the slides were washed three times for 5 min in PBS and blocked for 45 min using 12% bovine serum albumin (BSA; SigmaAldrich, A7030) or the Biotin/Avidin kit (PEG staining; Abcam, ab64212). After another washing step, primary antibodies were incubated at 4 °C overnight in a humidity chamber. Samples were washed thoroughly in PBS and then incubated with the secondary antibodies for 1 h in a humidity chamber. After incubation, sections were rewashed thoroughly in PBS. Finally, sections were mounted in a DAPI (Prolong Gold antifade reagent with DAPI; Invitrogen, P36935) mounting medium to counterstain nuclei. Matched images were taken with the same exposure and were processed and analyzed identically with the Axioscope 5 (Zeiss, Germany).

The primary antibodies used were PEG (1:100, Abcam, ab53449), CD31 (1:100, Abcam, ab28364), αSMA (1:100, Progen Biotechnik, BK61501), Collagen1A1 (1:100, BioRad, 2150-1410), F4/80 (1:100, Abcam, ab111101), CD206 (1:100, Acris, SM1857P), and VEGFR2 (1:20, R&D Systems, AF644). As secondary antibodies Alexa Fluor 488 (1:200, Invitrogen, A21208) was used for Collagen1A1, CD206, and VEGFR2 staining. For F4/80 stainings, Alexa Fluor 594 (1:200, Invitrogen, A21207) was used. Cy2 (016-220-084) was used for PEG and αSMA, and Cy5 (712-175-153) for CD31 stainings (1:500, Dianova). The analysis of $TUNEL^+$ apoptotic cells was performed using the TUNEL kit from Roche (11 684 795 910).

In Vitro Uptake Studies: Hepa1.6 and Hep-55.1C cells were purchased from American Type Culture Collection (ATCC) and maintained under standard cultivation conditions (37 °C, 5% CO2) in Dulbecco's modified Eagle's medium (DMEM; *w*: 4.5 g L^{-1} Glucose, *w*: L-Glutamine, w/o: Sodium pyruvate, *w*: 3.7 g L^{-1} NaHCO3, PAN-Biotech, P04-03550) supplemented with 10% fetal bovine serum (FBS, PAN-Biotech, P40-37500) and 1% Penicillin-Streptomycin (SigmaAldrich, P4333). Cells were passaged when reaching confluency of 80% using Trypsin (Hepa1.6; Trypsin

EDTA+, Thermo Fisher Scientific, 25 300 096) or Accutase (Hep-55.1C; Gibco, A1110501). In all studies, cells were seeded into 12-well plates (Greiner Bio-one, Germany) with 0.1×10^6 cells/well and allowed to attach over 24 h. All experiments were performed with at least two technical and three biological replicates.

For the immunofluorescence imaging analysis of in vitro uptake studies, the cell lines Hepa1.6 and Hep-55.1C were seeded on coverslips (Thermo Scientific, Germany). The next day, cells were stimulated with 10×10^{-6} M forskolin (diluted in DMSO, Sigma-Aldrich, F6886) for another 24 h. Inhibitory studies were based on Macia et al. 2006 for Dynasore,[47] Vercauteren et al. 2010 for Genistein,[48] Yang et al. 2017 for nystatin,[28] or Dutta et al. 2012[49] for Pitstop2. Briefly, cells were washed three times with 1 mL of PBS, and 1 mL of media supplemented with the respective inhibitor was added. All inhibitors were diluted in DMSO. Controls were either nonsupplemented media or media supplemented with DMSO (AppliChem, A3672,0250). When combining forskolin with nystatin incubation, cells were first incubated with forskolin for 24 h, and after washing three times with 1 mL PBS, nystatin was added. After incubating each respective stimulant, cells were washed three times with 1 mL PBS, and 5×10^{-9} M of Cy5.5-labeled liposomes were added for 24 h. The next day, cells were washed thoroughly three times with 1 mL of PBS and fixed for 15 min with 4% paraformaldehyde (PFA; ThermoFisher, J19943.K2). After another washing step, the cells were mounted in DAPI to counterstain nuclei and kept at 4 °C until image acquisition.

For the flow cytometry analysis of in vitro uptake studies, the cells were pretreated with stimulants as described in the immunofluorescence imaging analysis. After incubating each respective stimulant, the cells were washed three times with 1 mL PBS, and 10×10^{-9} M of Cy7-labeled liposomes were added for 1 h. Then, the cells were washed three times with 1 mL PBS and 250 µL trypsin-EDTA was added for 3 min. The cells were harvested with 500 µL medium and centrifuged for 10 min, 12 000 g, 4 °C (Centrifuge 5242R, Eppendorf). The pellet was resuspended in 250 µL cold PBS. Cells were sorted with a fluorescent-activated cell sorting analyzer (FACS; BD FACSCanto II System). Using the FlowJo v10 software, single cells were gated, and the APC-Cy7 positive cells were calculated using the median of fluorescent intensity (MFI).

Statistics: All experiments were performed at least three times independently if not stated otherwise. Data were quantified using the software linked to the indicated instruments and validated in GraphPad Prism 9 (San Diego, CA, USA). Statistical significance was assessed using Student's *t*-test, OneWay, or TwoWay analyses of variance (ANOVAs) followed by multiple comparisons and Mann-Whitney tests wherever appropriate. Statistically significant differences were determined as described in the figure legends.

Supporting Information

Supporting Information is available from the Wiley Online Library or from the author.

Acknowledgements

The authors would like to thank E. Brandt and A. Beckers for technical assistance with intrahepatic surgery and supply of the Hep-55.1C cell line. The authors furthermore thank M. Weiler for the preparation of liposomes. The authors gratefully acknowledge financial support from the German Research Foundation (DFG: GRK 2375 (Project No. 331065168)), the European Research Council (ERC: Meta-Targeting (Project No. 864121)), the German Research Foundation CRC1382 (Project-ID 403224013) to MH and CT, as well as DFG HA 7246/2-1 and Tr 285/10-2.

Open access funding enabled and organized by Projekt DEAL.

Conflict of Interest

The authors declare no conflict of interest.

Author Contributions

S.B. and J.M. contributed equally to this work. S.B. designed and S.B. and J.M. performed the experiments, analyzed the data, and wrote the manuscript. Q.W., H.S., L.S.C., and M.L.B. supported intrahepatic surgery. S.B., J.M., and Q.W. analyzed the data and performed the fasting of the mice. J.M. performed the TPLSM microscopy. J.M., D.M., (...), I.B., and J.N.M. performed i.v. injections and supported imaging experiments. D.M. and I.B. designed the TME analysis. I.B., J.N.M., T.L., and C.T. reviewed and edited the manuscript. M.H., C.T., and T.L. supervised the project. T.L. and C.T. conceived and coordinated the project.

Data Availability Statement

The data that support the findings of this study are available from the corresponding author upon reasonable request.

Keywords

cancer, chemotherapy, drug delivery, fasting, hepatocellular carcinoma, nanomedicine

Received: December 21, 2022
Revised: June 18, 2023
Published online: June 27, 2023

[1] G. Salvadori, F. Zanardi, F. Iannelli, R. Lobefaro, C. Vernieri, V. D. Longo, *Cell Metab.* **2021**, *33*, 2247.
[2] I. Caffa, V. Spagnolo, C. Vernieri, F. Valdemarin, P. Becherini, M. Wei, S. Brandhorst, C. Zucal, E. Driehuis, L. Ferrando, F. Piacente, A. Tagliafico, M. Cilli, L. Mastracci, V. G. Vellone, S. Piazza, A. L. Cremonini, R. Gradaschi, C. Mantero, M. Passalacqua, A. Ballestrero, G. Zoppoli, M. Cea, A. Arrighi, P. Odetti, F. Monacelli, G. Salvadori, S. Cortellino, H. Clevers, F. De Braud, et al., *Nature* **2020**, *583*, 620.
[3] C. Vernieri, G. Fucà, F. Ligorio, V. Huber, A. Vingiani, F. Iannelli, A. Raimondi, D. Rinchai, G. Frigè, A. Belfiore, L. Lalli, C. Chiodoni, V. Cancila, F. Zanardi, A. Ajazi, S. Cortellino, V. Vallacchi, P. Squarcina, A. Cova, S. Pesce, P. Frati, R. Mall, P. A. Corsetto, A. M. Rizzo, C. Ferraris, S. Folli, M. C. Garassino, G. Capri, G. Bianchi, M. P. Colombo, et al., *Cancer Discov.* **2022**, *12*, 90.
[4] S. de Groot, R. T. Lugtenberg, D. Cohen, M. J. P. Welters, I. Ehsan, M. P. G. Vreeswijk, V. T. H. B. M. Smit, H. de Graaf, J. B. Heijns, J. E. A. Portielje, A. J. van de Wouw, A. L. T. Imholz, L. W. Kessels, S. Vrijaldenhoven, A. Baars, E. M.-K. Kranenbarg, M. D. Carpentier, H. Putter, J. J. M. van der Hoeven, J. W. R. Nortier, V. D. Longo, H. Pijl, J. R. Kroep, *Nat. Commun.* **2020**, *11*, 3083.
[5] S. Di Biase, V. D. Longo, *Mol. Cell. Oncol.* **2016**, *3*, e1117701.
[6] N. M. Anderson, M. C. Simon, *Curr. Biol.* **2020**, *30*, R921.
[7] D. Rosenblum, N. Joshi, W. Tao, J. M. Karp, D. Peer, *Nat. Commun.* **2018**, *9*, 1410.
[8] R. J. DeBerardinis, N. S. Chandel, *Nat. Metab.* **2020**, *2*, 127.
[9] C. Lee, L. Raffaghello, S. Brandhorst, F. M. Safdie, G. Bianchi, A. Martin-Montalvo, V. Pistoia, M. Wei, S. Hwang, A. Merlino, L. Emionite, R. de Cabo, V. D. Longo, *Sci. Transl. Med.* **2012**, *4*, 124ra27.
[10] S. de Groot, H. Pijl, J. J. M. van der Hoeven, J. R. Kroep, *J. Exp. Clin. Cancer Res.* **2019**, *38*, 209.
[11] A. Nencioni, I. Caffa, S. Cortellino, V. D. Longo, *Nat. Rev. Cancer.* **2018**, *18*, 707.
[12] G. Mattheolabakis, C. M. Mikelis, *Front. Oncol.* **2019**, *9*, 1227.
[13] M. A. Miller, Y.-R. Zheng, S. Gadde, C. Pfirschke, H. Zope, C. Engblom, R. H. Kohler, Y. Iwamoto, K. S. Yang, B. Askevold, N.

Kolishetti, M. Pittet, S. J. Lippard, O. C. Farokhzad, R. Weissleder, *Nat. Commun.* **2015**, *6*, 8692.
[14] X. He, Y. Yang, L. Li, P. Zhang, H. Guo, N. Liu, X. Yang, F. Xu, *Drug Discov. Today.* **2020**, *25*, 1727.
[15] S. Yang, C. Cai, H. Wang, X. Ma, A. Shao, J. Sheng, C. Yu, *Cell Commun. Signal.* **2022**, *20*, 26.
[16] L. J. Havrilesky, M. Reiner, P. K. Morrow, H. Watson, J. Crawford, *Crit. Rev. Oncol. Hematol.* **2015**, *93*, 203.
[17] A. Bakrania, G. Zheng, M. Bhat, *Pharmaceutics* **2021**, *14*, 41.
[18] C. Yoo, K. Kim, J. H. Jeong, I. Kim, M. J. Kang, J. Cheon, B. W. Kang, H. Ryu, J. S. Lee, K. W. Kim, G. K. Abou-Alfa, B.-Y. Ryoo, *Lancet Oncol.* **2021**, *22*, 1560.
[19] S. Daher, M. Massarwa, A. A. Benson, T. Khoury, *J. Clin. Transl. Hepatol.* **2018**, *6*, 69.
[20] J. M. Llovet, R. K. Kelley, A. Villanueva, A. G. Singal, E. Pikarsky, S. Roayaie, R. Lencioni, K. Koike, J. Zucman-Rossi, R. S. Finn, *Nat. Rev. Dis. Primer.* **2021**, *7*, 6.
[21] W. Y. Tak, S.-M. Lin, Y. Wang, J. Zheng, A. Vecchione, S. Y. Park, M. H. Chen, S. Wong, R. Xu, C.-Y. Peng, Y.-Y. Chiou, G.-T. Huang, J. Cai, B. J. J. Abdullah, J. S. Lee, J. Y. Lee, J.-Y. Choi, J. Gopez-Cervantes, M. Sherman, R. S. Finn, M. Omata, M. O'Neal, L. Makris, N. Borys, R. Poon, R. Lencioni, *Clin. Cancer Res.* **2018**, *24*, 73.
[22] M. Hatting, A. K. Rines, C. Luo, M. Tabata, K. Sharabi, J. A. Hall, F. Verdeguer, C. Trautwein, P. Puigserver, *Cell Metab.* **2017**, *25*, 428.
[23] L. C. D. Pomatto-Watson, M. Bodogai, O. Bosompra, J. Kato, S. Wong, M. Carpenter, E. Duregon, D. Chowdhury, P. Krishna, S. Ng, E. Ragonnaud, R. Salgado, P. Gonzalez Ericsson, A. Diaz-Ruiz, M. Bernier, N. L. Price, A. Biragyn, V. D. Longo, R. de Cabo, *Nat. Commun.* **2021**, *12*, 6201.
[24] M. Weng, W. Chen, X. Chen, H. Lu, Z. Sun, Q. Yu, P. Sun, Y. Xu, M. Zhu, N. Jiang, J. Zhang, J. Zhang, Y. Song, D. Ma, X. Zhang, C. Miao, *Nat. Commun.* **2020**, *11*, 1869.
[25] P. M. Glassman, J. W. Myerson, L. T. Ferguson, R. Y. Kiseleva, V. V. Shuvaev, J. S. Brenner, V. R. Muzykantov, *Adv. Drug Delivery Rev.* **2020**, *157*, 96.
[26] A. Mantovani, P. Allavena, F. Marchesi, C. Garlanda, *Nat. Rev. Drug Discovery* **2022**, *21*, 799.
[27] B. Wahlang, C. McClain, S. Barve, L. Gobejishvili, *Cell. Signal.* **2018**, *49*, 105.
[28] Z. Yang, F. Wu, H. Yang, P. Zhou, *RSC Adv.* **2017**, *7*, 41779.
[29] Y. Zhang, M. Toneri, H. Ma, Z. Yang, M. Bouvet, Y. Goto, N. Seki, R. M. Hoffman, *J. Cell. Biochem.* **2016**, *117*, 2546.
[30] U. Ruman, S. Fakurazi, M. J. Masarudin, M. Z. Hussein, *Int. J. Nanomedicine.* **2020**, *15*, 1437.
[31] K. N. Phoenix, F. Vumbaca, M. M. Fox, R. Evans, K. P. Claffey, *Breast Cancer Res. Treat.* **2010**, *123*, 333.
[32] M. E. Levine, J. A. Suarez, S. Brandhorst, P. Balasubramanian, C.-W. Cheng, F. Madia, L. Fontana, M. G. Mirisola, J. Guevara-Aguirre, J. Wan, G. Passarino, B. K. Kennedy, M. Wei, P. Cohen, E. M. Crimmins, V. D. Longo, *Cell Metab.* **2014**, *19*, 407.
[33] S. Brandhorst, M. Wei, S. Hwang, T. E. Morgan, V. D. Longo, *Exp. Gerontol.* **2013**, *48*, 1120.
[34] E. Henke, R. Nandigama, S. Ergün, *Front. Mol. Biosci.* **2020**, *6*, 160.
[35] P. P. Provenzano, D. R. Inman, K. W. Eliceiri, J. G. Knittel, L. Yan, C. T. Rueden, J. G. White, P. J. Keely, *BMC Med.* **2008**, *6*, 11.
[36] M.-J. Luo, S.-S. Rao, Y.-J. Tan, H. Yin, X.-K. Hu, Y. Zhang, Y.-W. Liu, T. Yue, L.-J. Chen, L. Li, Y.-R. Huang, Y.-X. Qian, Z.-Z. Liu, J. Cao, Z.-X. Wang, Z.-W. Luo, Y.-Y. Wang, K. Xia, S.-Y. Tang, C.-Y. Chen, H. Xie, *Theranostics* **2020**, *10*, 3779.
[37] K. Welén, K. Jennbacken, T. Tesăn, J.-E. Damber, *Prostate Cancer Prostatic Dis.* **2009**, *12*, 41.
[38] P. V. Dickson, J. B. Hamner, T. L. Sims, C. H. Fraga, C. Y. C. Ng, S. Rajasekeran, N. L. Hagedorn, M. B. McCarville, C. F. Stewart, A. M. Davidoff, *Clin. Cancer Res.* **2007**, *13*, 3942.
[39] R. van der Meel, E. Sulheim, Y. Shi, F. Kiessling, W. J. M. Mulder, T. Lammers, *Nat. Nanotechnol.* **2019**, *14*, 1007.
[40] E. Blanco, H. Shen, M. Ferrari, *Nat. Biotechnol.* **2015**, *33*, 941.
[41] F. M. Safdie, T. Dorff, D. Quinn, L. Fontana, M. Wei, C. Lee, P. Cohen, V. D. Longo, *Aging* **2009**, *1*, 988.
[42] C. Lee, V. D. Longo, *Oncogene* **2011**, *30*, 3305.
[43] T. Wirtz, E. Brandt, P. Fischer, C. Holland, A. Röth, M. Baues, J.-N. May, J. Koehncke, T. Ritz, T. Lammers, T. Longerich, C. Trautwein, M.-L. Berres, *Gastroenterol.* **2022**, *60*, 34.
[44] I. Biancacci, F. De Lorenzi, B. Theek, X. Bai, J. May, L. Consolino, M. Baues, D. Moeckel, F. Gremse, S. Stillfried, A. El Shafei, K. Benderski, A. Azadkhah Shalmani, A. Wang, J. Momoh, Q. Peña, E. M. Buhl, J. Buyel, W. Hennink, F. Kiessling, J. Metselaar, Y. Shi, T. Lammers, *Adv. Sci.* **2022**, *9*, 2103745.
[45] M. Bartneck, K. M. Scheyda, K. T. Warzecha, L. Y. Rizzo, K. Hittatiya, T. Luedde, G. Storm, C. Trautwein, T. Lammers, F. Tacke, *Biomaterials* **2015**, *37*, 367.
[46] I. E. Allijn, B. M. S. Czarny, X. Wang, S. Y. Chong, M. Weiler, A. E. da Silva, J. M. Metselaar, C. S. P. Lam, G. Pastorin, D. P. V. de Kleijn, G. Storm, J.-W. Wang, R. M. Schiffelers, *J. Controlled Release.* **2017**, *247*, 127.
[47] E. Macia, M. Ehrlich, R. Massol, E. Boucrot, C. Brunner, T. Kirchhausen, Dynasore, *Cell-Permeable Inhibitor of Dynamin Dev. Cell.* **2006**, *10*, 839.
[48] D. Vercauteren, R. E. Vandenbroucke, A. T. Jones, J. Rejman, J. Demeester, S. C. De Smedt, N. N. Sanders, K. Braeckmans, *Mol. Ther.* **2010**, *18*, 561.
[49] D. Dutta, C. D. Williamson, N. B. Cole, J. G. Donaldson, *PLoS One* **2012**, *7*, e45799.